Numerical Assessment of Turbulent Forced Convection Heat Transfer Through Concentric Tube Heat Exchanger

Imad M. Salman
Midland Refineries Company, Al-Daura Refinery, Baghdad, Iraq

[1]*Received: 02/04/2026; Accepted: 25/04/2026; Published: 05/05/2026*

Abstract

In the present research, a numerical theoretical analysis of forced convection heat transfer in an imperfectly evolving turbulent flow in a centered annular channel is carried out. The study consisted of creating a mathematical model to perform numerical solution of the mass, momentum, and energy equations and two turbulence model equations of k-θ model by finite difference method (FDM). A program was developed in Fortran 95 language for numerical solution. The numerical calculations have been carried out for the air as the working fluid, which is utilized through a centered annular channel. The outer cylinder diameter was (Do = 177.8 mm), the inner cylinder diameter was (Di = 101.6 mm), and the annular channel length was (L = 35Dh). After heating the outer cylinder wall with constant flux condition, it was heated with constant temperature condition as well. In both cases inner cylinder was stationary and rotating at a certain speed, the wall of inner cylinder has been thermally insulated. The results showed an increase in the length of the hydrodynamic and thermal ingress with increasing Reynolds number. The Nusselt number levels of the heating condition with a constant heat flux are greater than that of the heating condition with a constant temperature condition. Rotation of the inner cylinder leads to a flattening of the axial velocity curve, and leads to an increase in the coefficient of friction and a clear increase in turbulent kinetic energy near the wall of the inner cylinder. Rotation also leads to an increase in the Nusselt number and a decrease in the wall temperature for the heating condition using a constant heat flux, and an increase in the overall heating condition using a constant wall temperature.

Keywords: *Heat Transfer; Heat exchanger; CFD; Nussellt number; Turbulent flow.*

1. Introduction

The phenomenon of convection heat transfer in eccentric annuli has garnered significant scholarly attention in recent years. This heightened interest is primarily attributable to the occurrence of eccentricity in mechanical devices, electrical motors, and generators, which frequently contributes to design tolerances and manufacturing constraints. Additional applications encompass the drilling and completion processes of oil wells, the heat exchanger industry, and the thermal insulation of buried conduits for district heating and cooling systems of subterranean electrical cables. Given that an annulus comprises two surfaces upon which thermal conditions may be specified independently, a multitude of heat transfer problems of considerable relevance arise. Several years' prior, Reynolds et al. [1] comprehensively addressed the issue of heat transfer in fully developed laminar flow within concentric annuli. They discerned that under typical assumptions, the energy equation exhibits linear characteristics. Consequently, a temperature distribution that adheres to arbitrary boundary conditions could be ascertained by merely superimposing suitable multiples of temperature distributions that conform to specific fundamental boundary conditions. Four fundamental boundary conditions were established, and the temperature distributions that satisfy these conditions were

[1] [1] *How to cite the article:* Salman I.M.; Numerical Assessment of Turbulent Forced Convection Heat Transfer Through Concentric Tube Heat Exchanger; *International Journal of Advances in Engineering Research*, May 2026, Vol 31, Issue 5; pg: 1-16

termed fundamental solutions. Maybe the first problem that was realized amongst other issues The single cylinder fluid flow and heat transfer [2–5] In all of these work the flow was only close to being fully laminar free convection heat transfer. Analytic approach for Ref. [6], Assumption of laminar fully developed f low is assumed for free convection case. The evolution of flow and heat transfer in concentric annulus has been investigated both numerically [7, 8] and experimentally [9].

Several authors dealt with the eccentric annulus which is part of the problem of advancing this knowledge about the phenomenon. Generally, the major portion of research associated with this topic has been performed using numerical and/or analytical techniques which have held back a moderate number of exploratory investigations. Hence, further experimental studies one of the aims of which is to gain insight into the physics of the problem, as regarded here will be valuable. One of the earliest contributions for eccentric annuli may be work by Heyda [10], who obtained flow profile from solution to momentum equation. An approximate solution to laminar forced convection in eccentric annuli with a large range of eccentricities and radius ratios has been given by Trombetta [11]. The counting was done with different eccentricities and radius ratio in the Nusselt number. He focused on hydro-dynamically and thermally fully developed flows. He worked out primitive solutions of the 1st, 2nd and 4th kind. Cheng and Hwang [12] provided a numerical solution for fully developed laminar flow with constant heat sources in eccentric annular ducts subjected to uniform heat flux from each wall. Also revealed by a numerical solution to the problem was the principle of maximum-flow-rate induction by free convection [13,14]. More studies showed that an optimum euthy(εu) exists at which e minimum solution the total heat transfer coefficient can be achieved [7,14]. The models give a fast solution to the following behaviors along the developing velocity profiles, axial variation of pressure and heat transfer parameters [15]. They assumed we have one of the annulus tubes at constant temperature and other insulated as thermal boundary conditions.

In this work, we undertake an in-depth numerical study of developing turbulent forced convection heat transfer for the flow of water within a circular concentric annulus, focusing on axial developments of local thermal hydraulic parameters and distinctly different outer and inner wall behavior. In contrast to fully-developed annular flow studies, the present work captures velocity, turbulence and thermal boundary-layer development as a result of more realistic inlet conditions, offering better insight into annular heat-transfer behavior.

2. Physical Models and Numerical Methods

The fluid flows perpendicularly on the pipe's cross-section as seen in Fig. 1. When the fluid enters the pipe from a large ambient space, zero flow boundary layer and thermal boundary layer peels off at pipe wall and meet together in center symmetry plane of the pipe. The overlap of the velocity boundary layer and thermal boundary layer shows that inside the pipeline, flow and heat transfer have fully developed. At this point on, his local surface heat transfer coefficient is almost constant. The region included between the entrance segment and completely created portion is distinguished as the Entrance section. As the flow develops to some degree, strong perturbations and dynamics of fluid micro-clusters make effect of entrance section gradually become weak. The aim of the study and to remove any influence from the entrance section, but also since we are using forced flow where entrances limited heat transfer occurs a 100 de long experimental pipe section (l= 100de) was used in this research. de is the characteristic length for calculation of heat-transfer Nusselt Number, specifically the equivalent diameter. For circular pipes, the equivalent diameter is considered to be equal to diameter of round pipe. The equivalent diameter for non-circular pipes is determined according to the following direction: de=4Ac/P, where Ac = Flow cross-sectional area of pipeline; P= Wetted perimeter or length of contact surface between pipe wall and fluid. Fig. 1: Physical Model and Meshing (not to scale) Some other assumptions made in this paper, apart from the physical models described above include: working fluid is a Newtonian fluid; radiation free; gravity and body forces are neglected.

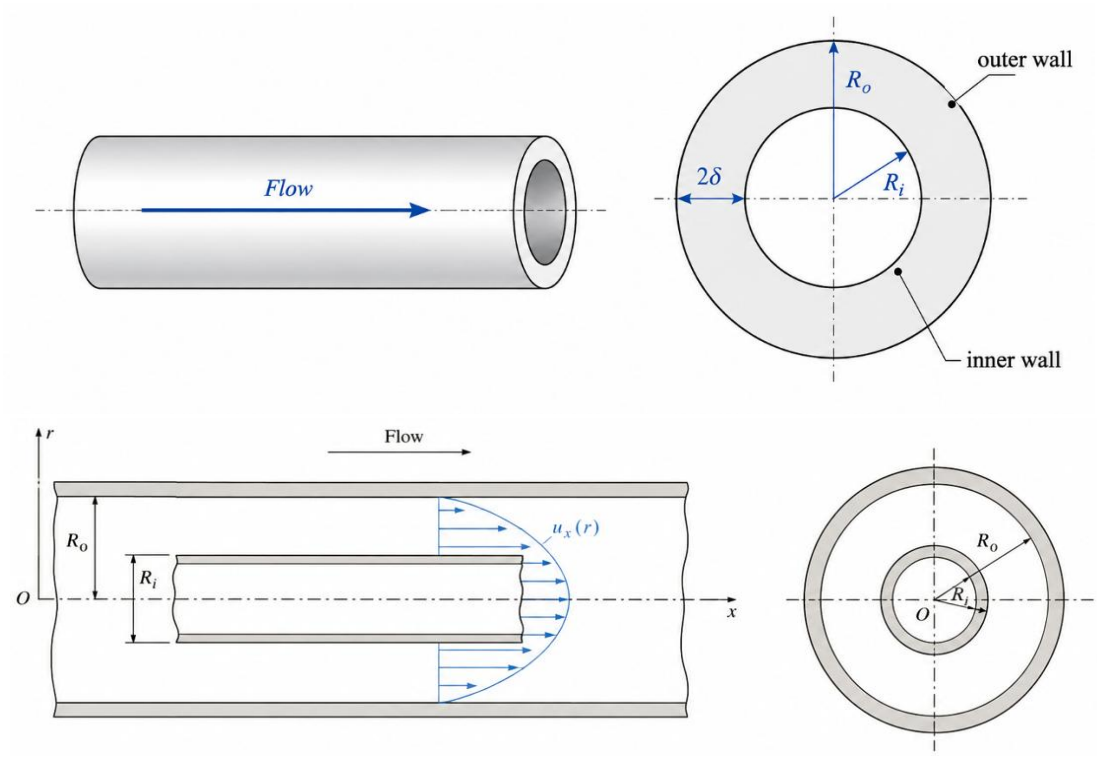

Fig. 1. Physical geometry of the concentric annulli.

2.1 Mathematical Modelling

- Reynolds-averaged continuity equation

$$\frac{\partial U_i}{\partial x_i} = 0 \qquad (1)$$

where U_i is the time-averaged velocity component in the x_i direction.

- Reynolds-averaged momentum equation

$$\rho U_j \frac{\partial U_i}{\partial x_j} = -\frac{\partial P}{\partial x_i} + \frac{\partial}{\partial x_j}\left[\mu\left(\frac{\partial U_i}{\partial x_j} + \frac{\partial U_j}{\partial x_i}\right) - \rho\overline{u_i' u_j'}\right] \qquad (2)$$

where P is the mean pressure, ρ is the fluid density, μ is the dynamic viscosity, and u_i' and u_j' are fluctuating velocity components.

The Reynolds stress tensor is closed using the Boussinesq eddy-viscosity hypothesis:

$$-\rho\overline{u_i' u_j'} = \mu_t\left(\frac{\partial U_i}{\partial x_j} + \frac{\partial U_j}{\partial x_i}\right) - \frac{2}{3}\rho k\delta_{ij} \qquad (3)$$

where μ_t is the turbulent viscosity, k is the turbulent kinetic energy, and δ_{ij} is the Kronecker delta.

Using this closure, the momentum equation may also be expressed in terms of the effective viscosity as:

$$\rho U_j \frac{\partial U_i}{\partial x_j} = -\frac{\partial}{\partial x_i}\left(P + \frac{2}{3}\rho k\right) + \frac{\partial}{\partial x_j}\left[(\mu + \mu_t)\left(\frac{\partial U_i}{\partial x_j} + \frac{\partial U_j}{\partial x_i}\right)\right] \quad (4)$$

- **Turbulent viscosity**

The turbulent viscosity is calculated as:

$$\mu_t = \rho C_\mu \frac{k^2}{\varepsilon} \quad (5)$$

where ε is the turbulent dissipation rate.

- **Transport equation for turbulent kinetic energy**

The transport equation of turbulent kinetic energy is given by:

$$\rho U_j \frac{\partial k}{\partial x_j} = \frac{\partial}{\partial x_j}\left[\left(\mu + \frac{\mu_t}{\sigma_k}\right)\frac{\partial k}{\partial x_j}\right] + P_k - \rho\varepsilon \quad (6)$$

The production term P_k is defined as:

$$P_k = -\rho\overline{u_i{}' u_j{}'}\frac{\partial U_i}{\partial x_j} \quad (7)$$

or, using the mean strain-rate tensor:

$$P_k = 2\mu_t S_{ij} S_{ij} \quad (8)$$

with

$$S_{ij} = \frac{1}{2}\left(\frac{\partial U_i}{\partial x_j} + \frac{\partial U_j}{\partial x_i}\right) \quad (10)$$

- **Transport equation for turbulent dissipation rate**

The dissipation-rate equation is expressed as:

$$\rho U_j \frac{\partial \varepsilon}{\partial x_j} = \frac{\partial}{\partial x_j}\left[\left(\mu + \frac{\mu_t}{\sigma_\varepsilon}\right)\frac{\partial \varepsilon}{\partial x_j}\right] + C_{\varepsilon 1}\frac{\varepsilon}{k}P_k - C_{\varepsilon 2}\rho\frac{\varepsilon^2}{k} \quad (11)$$

Turbulence model constants are listed in Table 1.

Table 1 k-ε turbulence model constants.

Constant	Standard value
C_μ	0.09
$C_{\varepsilon 1}$	1.44
$C_{\varepsilon 2}$	1.92
σ_k	1.00
σ_ε	1.30

- **Energy equation for turbulent forced convection**

For turbulent heat transfer, the Reynolds-averaged energy equation can be written as:

$$\rho c_p U_j \frac{\partial T}{\partial x_j} = \frac{\partial}{\partial x_j}\left[\left(\lambda + \frac{\mu_t c_p}{\mathrm{Pr}_t}\right)\frac{\partial T}{\partial x_j}\right] \quad (12)$$

In the above equation, T denotes the mean temperature, c_p the specific heat, λ the thermal conductivity, and Pr_t the turbulent Prandtl number. When performing air-flow heat-transfers with computer simulation, Pr_t is typically set at about 0.85–0.90.

- **Wall-function treatment**

In the conventional wall-function method, the viscous sublayer is not explicitly solved. On the contrary, the first near wall computational node is located in the logarithmic part of the turbulent boundary layer. This approach allows the mesh size to be decreased close to the wall and still provides good predictions of the wall shear stress and turbulent heat transfer for high Reynolds number flows.

- **Dimensionless wall distance**

The non-dimensional wall distance is defined as:

$$\mathbf{y^+ = \rho\, u\tau\, y_P / \mu} \quad (13)$$

where y_P is the normal distance from the wall to the first cell center and u_τ is the friction velocity:

$$u_\tau = \sqrt{\frac{\tau_w}{\rho}} \quad (14)$$

where τ_w is the wall shear stress.

- **Dimensionless velocity**

The non-dimensional velocity is expressed as:

$$U^+ = UP / u\tau \quad (14)$$

where U_P is the mean velocity parallel to the wall at the first near-wall cell center.

For the logarithmic layer, the law of the wall is applied as:

$$U^+ = (1/\kappa)\ln(E\, y^+) \quad (15)$$

where κ is the von Karman constant and E is an empirical wall-function coefficient:
$\kappa = 0.41, \quad E = 9.793$

The wall shear stress is then obtained from:

$$\tau_w = \rho u_\tau^2 \quad (16)$$

- **Near-wall treatment of k and epsilon**

The turbulent kinetic energy at the wall-adjacent cell is commonly prescribed a zero normal-gradient condition for the standard k–ε model with wall functions:

$$\frac{\partial k}{\partial n} = 0 \quad (17)$$

where n is the wall-normal direction.

The dissipation rate at the wall next to the cell is estimated using the local-equilibrium assumption:

$$\varepsilon_P = \frac{C_\mu^{3/4} k_P^{3/2}}{\kappa y_P} \quad (18)$$

The mean turbulent kinetic energy, k_P and dissipation rate, ε_P, are at the near-wall cell center. The near-wall generation of turbulent kinetic energy can be expressed as:

$$P_{k,P} = \tau_w \left(\frac{\partial U}{\partial y}\right)_P \quad (19)$$

The near-wall production of turbulent kinetic energy may be written in a wall-function form as:

$$P_{k,P} = \tau_w \left(\frac{\partial U}{\partial y}\right)_P \quad (20)$$

At the location where the wall-normal velocity gradient is calculated using the logarithmic wall law.

The first near-wall node should typically be located at a distance of y^+, such that:

$30 < y^+ < 300$

This range will keep the center of the first cell within the region of turbulent boundary layer in a log region. The wall-function assumption is no longer valid if y^+ is too small, and if it is too large, the gradients in the boundary layer may not be well represented.

2.2 CFD modelling

The computational domain was defined as an axisymmetric annulus in the r−x plane, with x denoting the axial flow direction and r denoting the radial coordinate. Again, the region in one cross section extending from the inlet section at x=0 to the outlet section at x=L and in radial boundaries from inner radius R_i and outer radius R_o. It is also much more computationally cheap than a full 2D model and retains the primary axial (i.e., batch) and radial transport aspects of annular flow. A structured quadrilateral mesh for the computational domain was generated. Local mesh refinement was implemented close to the inner and outer walls in order to resolve a more accurate near-wall velocity and temperature gradients. This refinement is necessary especially due to the fact that large gradients in values occur near solid surfaces due to no-slip boundary condition. In the core flow region where the gradients are not very steep a comparatively coarse mesh was employed. The inlet and outlet boundaries were defined on left-hand side and the right-hand side of the domain, respectively, while a solid wall was assumed for both inner and outer surfaces. Figure 2 shows the computational grid model. There are a few assumptions above which can be summarized as:

The flow is turbulent and the fluid is incompressible. The source term Q in energy equation is constant. Let: (i) The wall temperature, T_w=0 (ii) The dimensionless wall temperature.

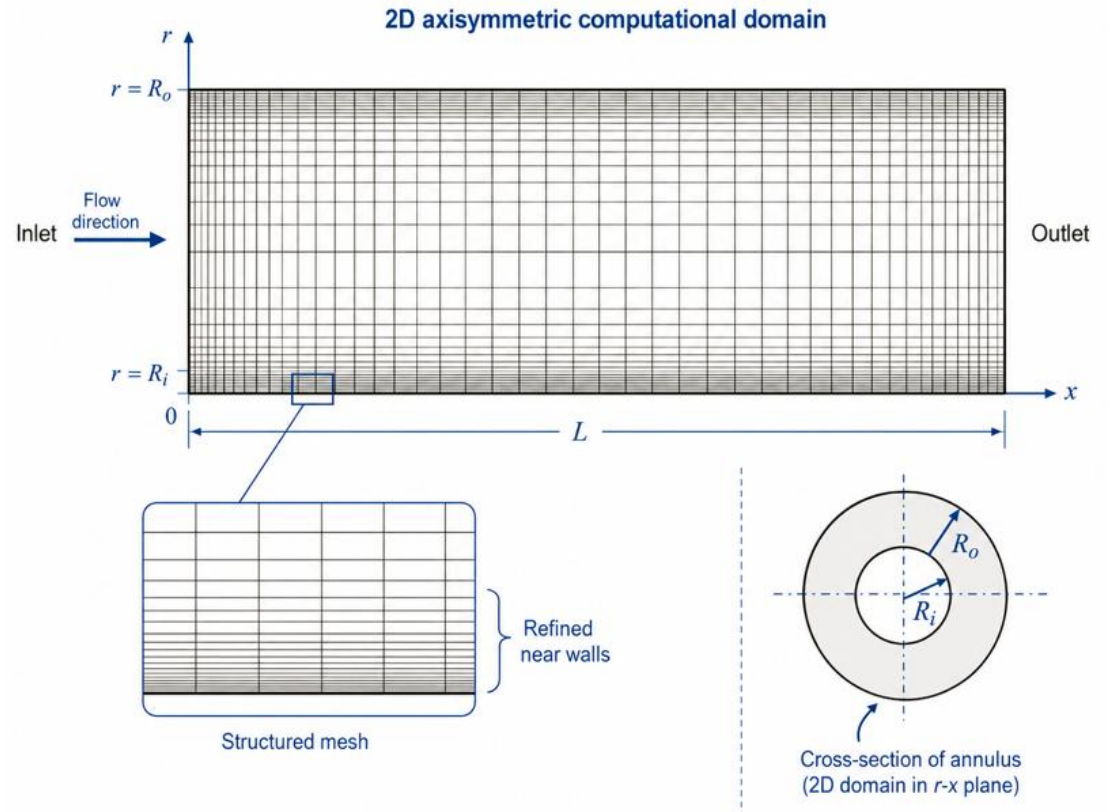

Figure 2 Two-dimensional axisymmetric computational mesh in the r−x plane for annular flow, showing the inlet, outlet, radial boundaries (Ri and Ro), axial length L, and near-wall mesh refinement.

The following equations are compact finite difference operator forms. The resulting equations are usually preferable to be written in this form because the operators have been defined explicitly in Table 2, and the equations are clear and readily implemented in a manuscript.

Table 2. Boundary conditions.

Boundary	Location	Velocity / Pressure Conditions	Turbulence Conditions	Thermal Condition	Finite-Difference Implementation
Inlet	x = 0	u = U_in v = 0	k = k_in ε = ε_in	$T = T_{in}$	$\varphi_{0,j} = \varphi_{in}$ where φ = u, k, ε, T
Outlet	x = L	∂u/∂x = 0 ∂v/∂x = 0 p = p_out or ∂p/∂x = 0	∂k/∂x = 0 ∂ε/∂x = 0	∂T/∂x = 0	$\varphi_{Nx,j} = \varphi_{Nx-1,j}$ where φ = u, v, k, ε, T
Inner wall	$r = R_i$	No penetration: v = 0 Axial velocity u is treated using wall functions instead of direct no-slip resolution.	∂k/∂r = 0 ε_P = C_μ^(3/4) k_P^(3/2) / (κ y_P)	Adiabatic: ∂T/∂r = 0 or constant temperature: $T = T_{w,i}$	$k_w = k_P$ Adiabatic wall: T_i,0 = T_i,1 Wall shear stress obtained from the logarithmic wall law.

Outer wall	$r = R_o$	No penetration: $v = 0$ Axial velocity u is treated using wall functions instead of direct no-slip resolution.	$\partial k/\partial r = 0$ $\varepsilon_p = C_\mu^{(3/4)} k_P^{(3/2)} / (\kappa y_P)$	Adiabatic: $\partial T/\partial r = 0$ or constant temperature: $T = T_{w,o}$	k_w = k_P Adiabatic wall: T_i,Nr = T_i,Nr−1 Wall shear stress obtained from the logarithmic wall law.
Annular fluid domain	$R_i \le r \le R_o$ $0 \le x \le L$	Flow is solved only within the annular passage.	k and ε are solved in the fluid region only.	Temperature is solved in the fluid region only.	Structured grid nodes: $x_i = i\,\Delta x$ $r_j = R_i + j\,\Delta r$

The inlet turbulence quantities may be estimated from turbulence intensity I and turbulence length scale ℓ as:

$k_{in} = 3/2\,(U_{in}\,I)^2$

$\varepsilon_{in} = C_\mu^{(3/4)}\, k_{in}^{(3/2)} / \ell$

For wall-function treatment, the first near-wall node should generally lie within the logarithmic region:

$30 < y^+ < 300$

$y^+ = \rho\, u_\tau\, y_P / \mu$

$U^+ = (1/\kappa)\ln(E\,y^+), \quad \kappa = 0.41, \quad E = 9.793$

If a low-Reynolds-number turbulence model or enhanced wall treatment is used, the near-wall mesh requirement changes and the first grid point should generally be placed at y^+ approximately equal to 1. Table 3 shows the finite difference equation for the governing equations.

Table 3 The finite difference equation for the governing equations.

Parameter	Finite difference equations
Continuity	$\frac{u_{i+1,j} - u_{i-1,j}}{2\Delta x} + \frac{v_{i,j+1} - v_{i,j-1}}{2\Delta r} + \frac{v_{i,j}}{r_j} = 0$
Axial momentum, u	$\rho C_u = -G_x + \mu_{\text{eff},i,j} D_u$ $C_u = u_{i,j}\frac{u_{i+1,j} - u_{i-1,j}}{2\Delta x} + v_{i,j}\frac{u_{i,j+1} - u_{i,j-1}}{2\Delta r}$ $G_x = \frac{p_{i+1,j} - p_{i-1,j}}{2\Delta x}$ $D_u = D_{u,x} + D_{u,r} + D_{u,a}$ $D_{u,x} = \frac{u_{i+1,j} - 2u_{i,j} + u_{i-1,j}}{\Delta x^2}$ $D_{u,r} = \frac{u_{i,j+1} - 2u_{i,j} + u_{i,j-1}}{\Delta r^2}$ $D_{u,a} = \frac{1}{r_j}\frac{u_{i,j+1} - u_{i,j-1}}{2\Delta r}$

Parameter	Finite difference equations
Radial momentum, v	$\rho C_v = -G_r + \mu_{\text{eff},i,j} D_v$ $C_v = u_{i,j} \frac{v_{i+1,j} - v_{i-1,j}}{2\Delta x} + v_{i,j} \frac{v_{i,j+1} - v_{i,j-1}}{2\Delta r}$ $G_r = \frac{p_{i,j+1} - p_{i,j-1}}{2\Delta r}$ $D_v = D_{v,x} + D_{v,r} + D_{v,a} - \frac{v_{i,j}}{r_j^2}$ $D_{v,x} = \frac{v_{i+1,j} - 2v_{i,j} + v_{i-1,j}}{\Delta x^2}$ $D_{v,r} = \frac{v_{i,j+1} - 2v_{i,j} + v_{i,j-1}}{\Delta r^2}$ $D_{v,a} = \frac{1}{r_j} \frac{v_{i,j+1} - v_{i,j-1}}{2\Delta r}$
Effective viscosity	$\mu_{\text{eff},i,j} = \mu + \mu_{t,i,j}$
Turbulent viscosity	$\mu_{t,i,j} = \rho C_\mu \frac{k_{i,j}^2}{\varepsilon_{i,j}}$
Turbulent kinetic energy, k	$\rho C_k = \Gamma_{k,i,j} D_k + P_{k,i,j} - \rho \varepsilon_{i,j}$ $C_k = u_{i,j} \frac{k_{i+1,j} - k_{i-1,j}}{2\Delta x} + v_{i,j} \frac{k_{i,j+1} - k_{i,j-1}}{2\Delta r}$ $D_k = D_{k,x} + D_{k,r} + D_{k,a}$ $D_{k,x} = \frac{k_{i+1,j} - 2k_{i,j} + k_{i-1,j}}{\Delta x^2}$ $D_{k,r} = \frac{k_{i,j+1} - 2k_{i,j} + k_{i,j-1}}{\Delta r^2}$ $D_{k,a} = \frac{1}{r_j} \frac{k_{i,j+1} - k_{i,j-1}}{2\Delta r}$
Dissipation rate, epsilon	$\rho C_\varepsilon = \Gamma_{\varepsilon,i,j} D_\varepsilon + C_{\varepsilon 1} \frac{\varepsilon_{i,j}}{k_{i,j}} P_{k,i,j} - C_{\varepsilon 2} \rho \frac{\varepsilon_{i,j}^2}{k_{i,j}}$ $C_\varepsilon = u_{i,j} \frac{\varepsilon_{i+1,j} - \varepsilon_{i-1,j}}{2\Delta x} + v_{i,j} \frac{\varepsilon_{i,j+1} - \varepsilon_{i,j-1}}{2\Delta r}$ $D_\varepsilon = D_{\varepsilon,x} + D_{\varepsilon,r} + D_{\varepsilon,a}$ $D_{\varepsilon,x} = \frac{\varepsilon_{i+1,j} - 2\varepsilon_{i,j} + \varepsilon_{i-1,j}}{\Delta x^2}$ $D_{\varepsilon,r} = \frac{\varepsilon_{i,j+1} - 2\varepsilon_{i,j} + \varepsilon_{i,j-1}}{\Delta r^2}$ $D_{\varepsilon,a} = \frac{1}{r_j} \frac{\varepsilon_{i,j+1} - \varepsilon_{i,j-1}}{2\Delta r}$

Parameter	Finite difference equations
Energy equation, T	$\rho c_p C_T = \Gamma_{T,i,j} D_T$ $C_T = u_{i,j} \frac{T_{i+1,j} - T_{i-1,j}}{2\Delta x} + v_{i,j} \frac{T_{i,j+1} - T_{i,j-1}}{2\Delta r}$ $D_T = D_{T,x} + D_{T,r} + D_{T,a}$ $D_{T,x} = \frac{T_{i+1,j} - 2T_{i,j} + T_{i-1,j}}{\Delta x^2}$ $D_{T,r} = \frac{T_{i,j+1} - 2T_{i,j} + T_{i,j-1}}{\Delta r^2}$ $D_{T,a} = \frac{1}{r_j} \frac{T_{i,j+1} - T_{i,j-1}}{2\Delta r}$
Diffusion coefficient for k	$\Gamma_{k,i,j} = \mu + \frac{\mu_{t,i,j}}{\sigma_k}$
Diffusion coefficient for epsilon	$\Gamma_{\varepsilon,i,j} = \mu + \frac{\mu_{t,i,j}}{\sigma_\varepsilon}$
Thermal diffusion coefficient	$\Gamma_{T,i,j} = \lambda + \frac{\mu_{t,i,j} c_p}{Pr_t}$

3. Results and Discussion

Figure 3 shows velocity profile in the axial direction are considered to show the hydrodynamic development stages of the adjacent layer for the different sections of the annular channel for Reynolds number (Re=20000). The effect of the viscous forces is noticeable and the neighboring layer increases with distance along the axis. We notice that the shape of the neighboring layer is constant beyond a certain distance from the inlet and this distance is known as the length. Figure 4 shows The effect of the rotation of the inner cylinder on the axial velocity curve at (Z+=35) and Reynolds number (20000) is demonstrated, in which we note that the axial velocity curve is lower than the same for a stationary inner cylinder due to the increased intensity of the eddy current caused by the rotation.

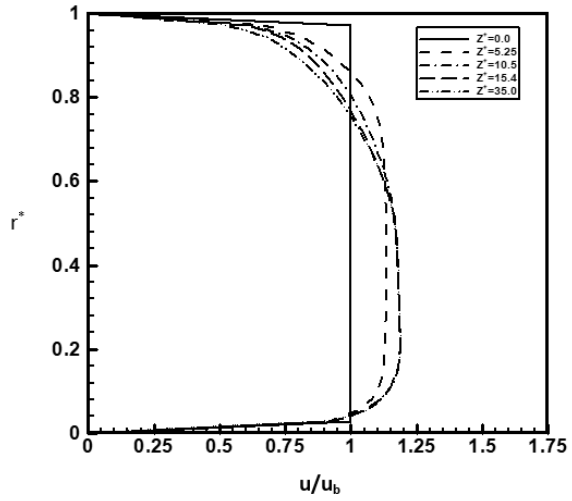

Figure 3 developing velocity profile in the axial direction.

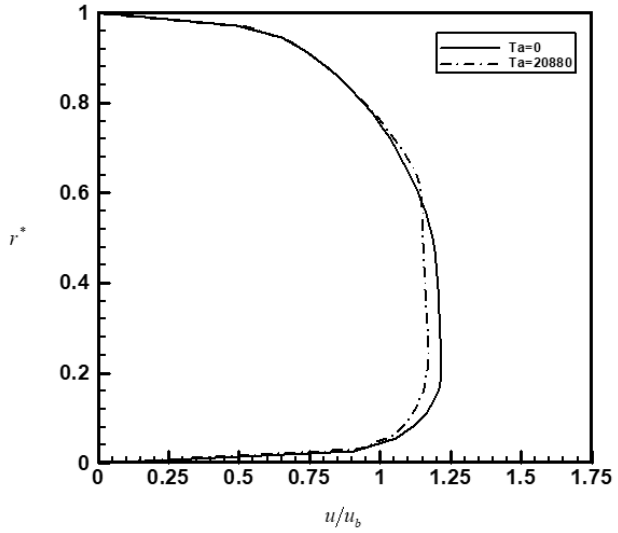

Figure 4 Effect of the rotation of the inner cylinder on the axial velocity.

Figure 5 shows the evolution of the dimensionless turbulent kinetic energy for the Reynolds numbers (20000) for a stationary inner cylinder. We observe that the maximum value of the turbulent kinetic energy is at the walls and it decreases in the central region of the annular cavity. The kinetic energy is greatest at the lowest velocity, near the walls. The significant decrease in the axial velocity near the outer wall is seen, which can be interpreted as the increase in kinetic energy near this wall. The turbulent kinetic energy decreases further in the central area of the annular cavity. In the figure 6, the turbulent viscosity is seen to increase with the increase of the Reynolds number Re for values of the Reynolds number (20000). Similar to the increase in the length required to reach the complete evolution with the increase of Reynolds number Re, an increasing length to reach the complete evolution with Re is also observed in the evolution of axial velocity and turbulent kinetic energy.

Figure 7 shows the development of Reynolds stress at seven different points for the Reynolds numbers (20000). It is seen that at the highest speed the Reynolds stress is zero at the maximum speed and the lowest Reynolds stress is near the inner wall while the highest Reynolds stress is near the outer wall at this speed. The values of Reynolds stress range between -0.4 and 0.4. The development deviation near the outer wall is very evident by the gradual slope in the speed curve near the outer wall. This is the same for other Reynolds numbers.

Figure 8 shows the axial development of the local friction coefficient for Reynolds numbers (20000-80000) for the case of a stationary inner cylinder at the inner and outer walls, respectively. It is seen that the local friction coefficient decreases with increasing Reynolds number Re (Reynolds number), because the turbulent kinetic energy included in the calculation of the shear stress, which is calculated by the wall function decreases, and also because the thickness of the adjacent layer decreases with increasing Reynolds number Re (Reynolds number), which in turn decreases the local friction coefficient.

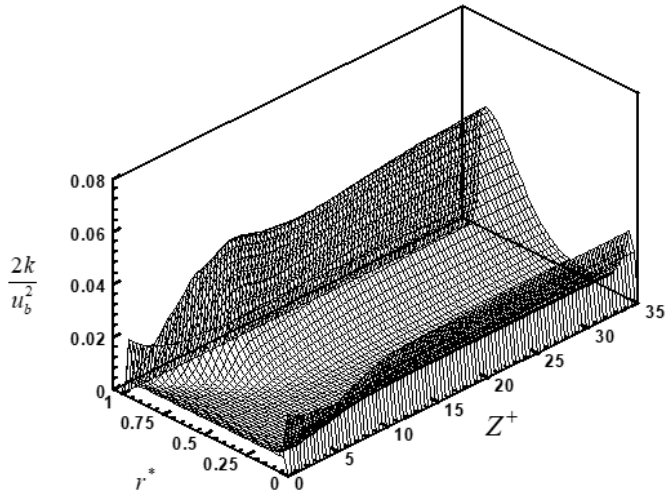

Figure 5 Developing in turbulent kinetic energy in axial direction.

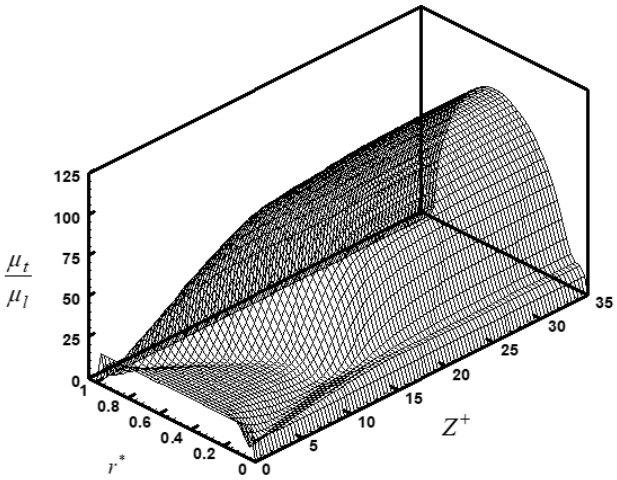

Figure 6 Developing turbulent viscosity in the axial direction.

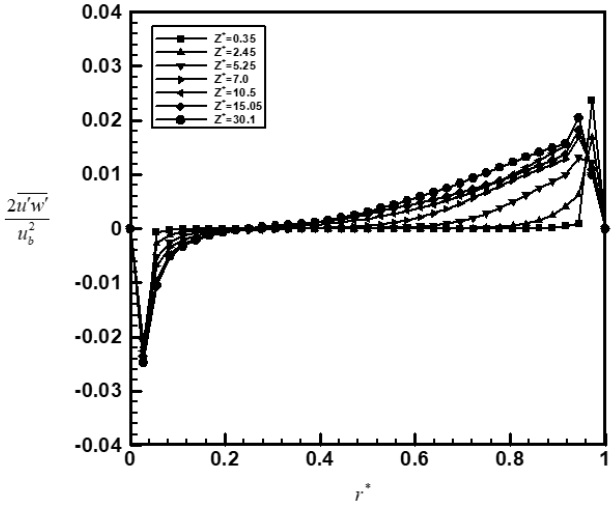

Figure 7 Development of Reynolds stress at seven different points.

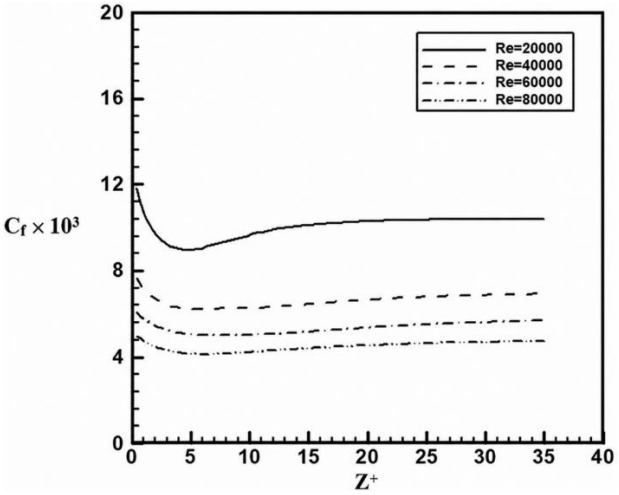

Figure 8 Axial development of the local friction coefficient for Reynolds numbers (20000-80000).

Figure 9 shows the evolution of temperature lines and contour for the case of the outer cylinder wall exposed to a uniform heat flux qo=500W/m^2 and the inner cylinder is stationary and for Reynolds numbers (20000), where the temperature starts to increase in the axial direction (in the direction of the flow), while in the diagonal direction we observe a gradual decrease in temperatures near the outer cylinder wall, and the decrease continues in the central region more significantly, and the decrease continues less sharply near the thermally insulated inner cylinder wall. The turbulent heat flux diagonal distribution for a stationary inner cylinder at different locations, corresponding to the Reynolds numbers (20000) is shown in Figure 10. This brings some added complexity in trying to describe these figures. The value of the turbulent heat flux reaches a peak close to the heated wall and is then reduced within the central part of the annular cavity. Next, it increases a small amount as we approach the thermally insulated inner wall and low mass tipping point back down. Figure 11 demonstrates the same axial evolution of the local Nusselt number for constant heat flux and constant temperature, as shown in figures(a)(b). Local Nusselt number axial variation for the constant heat flux (a) As we have, the Nusselt number is maximum at inlet Z+=0 and it diminishes to an almost constant value as approaching downstream. By the inlet region the neighboring layer is equal to 0 therefore, it gets a maximum convection heat transfer coefficient. For this reason, the evolution of the adjacent layer starts to grow and is associated with a decrease of H at an almost constant level.

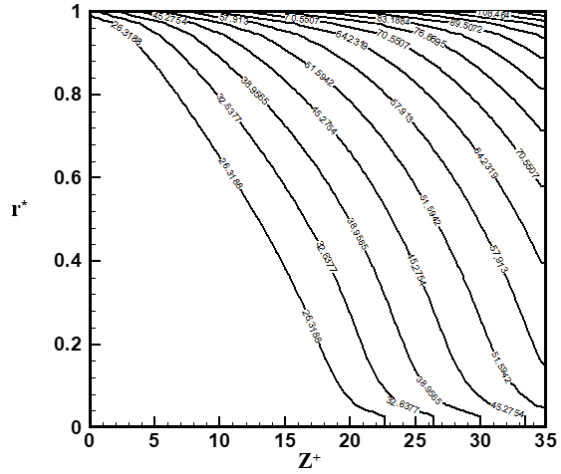

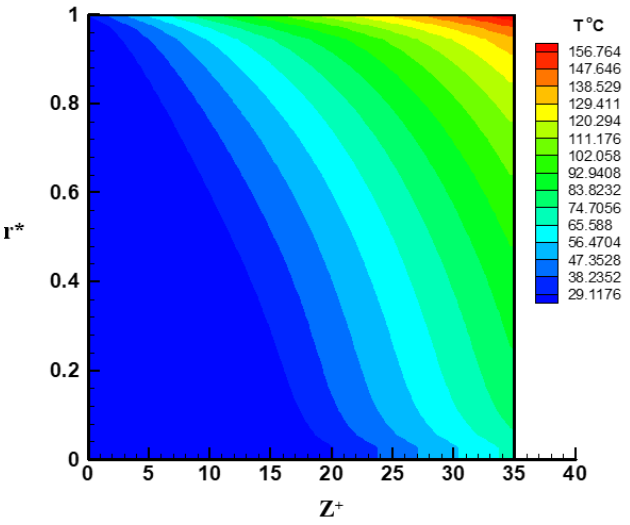

Figure 9 Temperature lines and contour for the case of the outer cylinder wall exposed to a uniform heat flux qo=500W/m^2.

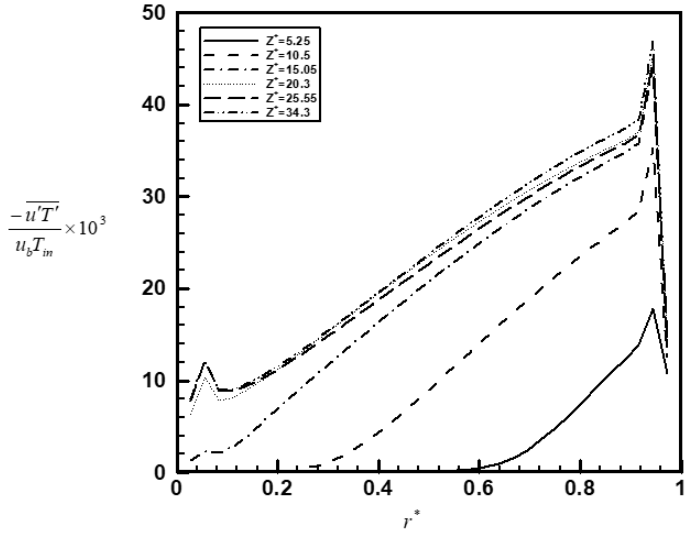

Figure 10 Diagonal distribution of the turbulent heat flux for Reynolds for a stationary inner cylinder at different locations.

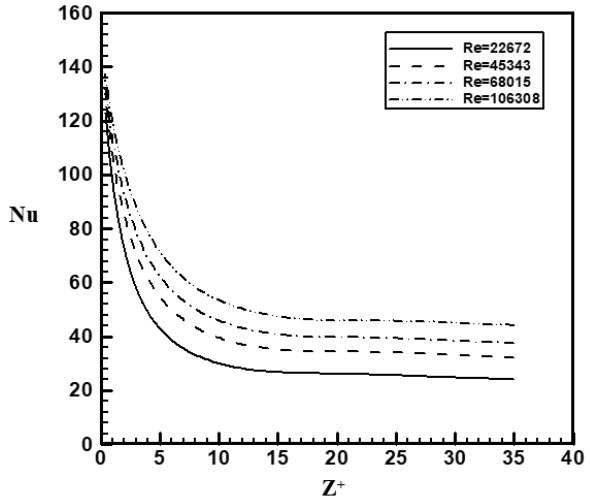

Figure 11 Axial evolution of the local Nusselt number for a constant inner cylinder.

4. Conclusions

Based on the results of the numerical solution of the present research for the cases of stationary and moving inner cylinder and for heating condition imposed by a constant heat flux condition applied for a certain length in the inlet, and constant temperature condition applied for another length in the inlet, the following conclusions are drawn:

i. The length of the hydrodynamic inlet required for the velocity curve to reach full development is increased with increasing Reynolds number.
ii. Increase Reynolds number results in a decrease in the thickness of the layer adjacent to the velocity curve, which explains the change in the plane of this curve.
iii. Away from the wall region, the level of turbulent kinetic energy reduces, and that of Reynolds stress reduces.
iv. The coefficient of local friction at the inner wall is greater than at the outer wall of the annular cavity and is also decreasing with the increase of Reynolds number.
v. Under the constant heat flux condition, the turbulent heat flux is the largest at the outer wall (heated wall) and the smallest is near the inner wall. The minimum Nusselt number level under the constant wall temperature condition is located in the center region of the annular cavity while this condition is lower under constant heat flux condition.

Conflict of Interest The authors declare that they have no conflict of interest.

Funding Declaration This research did not receive any specific grant from funding agencies in the public, commercial, or not-for-profit sectors.

References

Al-Arabi, M., El-Shaarawi, M. A. I., & Abdul Aziz, M. (1987). Natural convection in uniformly heated vertical annuli. *International Journal of Heat and Mass Transfer, 30*, 1381–1389.

Al-Arabi, M., Khamis, M., & Abdul Aziz, M. (1991). Heat transfer by natural convection from the inside surface of a uniformly heated tube at different angles of inclination. *International Journal of Heat and Mass Transfer, 34*, 1019–1025.

Cheng, K. C., & Hwang, G. (1968). Laminar forced convection in eccentric annuli. *AIChE Journal, 14*, 510–512.

Dyer, J. R. (1975). The development of laminar natural convection flow in a vertical uniform heat flux duct. *International Journal of Heat and Mass Transfer, 18*, 1455–1465.

El-Shaarawi, M. A. I., & Al-Nimr, M. A. (1990). Fully developed laminar natural convection in open-ended vertical concentric annuli. *International Journal of Heat and Mass Transfer, 33*, 1873–1884.

Elshazly, K., Moawed, M., Ibrahim, E., & Emara, M. (2005). Heat transfer by free convection from the inside surface of the vertical and inclined elliptic tube. *Energy Conversion and Management, 46*, 1443–1463.

Feldman, E. E., Hornbeck, R. W., & Osterle, J. F. (1982). A numerical solution of laminar developing flow in eccentric annular ducts. *International Journal of Heat and Mass Transfer, 25*, 231–241.

Heyda, J. F. (1959). A Green function solution for the laminar incompressible flow between non-concentric cylinders. *Journal of the Franklin Institute, 267*, 25–34.

Hosseini, R., Heyrani-Nobari, M. R., & Hatam, M. (2005). An experimental study of heat transfer in an open-ended vertical eccentric annulus with insulated and constant heat flux boundaries. *Applied Thermal Engineering, 25*, 1247–1257.

Jarral, S., & Campo, A. (2005). Experimental study of natural convection from electrically heated vertical cylinders immersed in air. *Experimental Heat Transfer, 18*, 127–134.

Lundberg, R. E., McCuen, P. A., & Reynolds, W. C. (1963). Heat transfer in annular passages: Hydrodynamically developed laminar flow with arbitrary prescribed wall temperatures or heat fluxes. *Journal of the Franklin Institute, 6*, 495–529.

Mokheimer, E. M. A., & El-Shaarawi, M. A. I. (2004). Developing mixed convection in vertical eccentric annuli. *Heat and Mass Transfer, 41*, 176–187.

Mokheimer, E. M. A., & El-Shaarawi, M. A. I. (2005). Maximum possible induced flow rates in open-ended vertical eccentric annuli with uniform heat flux. *International Journal of Numerical Methods for Heat & Fluid Flow, 15*, 161–182.

Reynolds, W. C., Lundberg, R. E., & McCuen, P. A. (1963). Heat transfer in annular passages. *International Journal of Heat and Mass Transfer, 6*, 483–529.

Trombetta, M. L. (1971). Laminar forced convection in eccentric annuli. *International Journal of Heat and Mass Transfer, 14*, 1161–1173.

About Author

Imad M. Salman is qualified engineer with a Bachelor of science degree from the University of Technology, Baghdad, earned in 1997. He has extensive experience in engineering inspection and project management within the oil refining industry, particularly with the Midland Refineries Company (MRC) at the Al-Daura Refinery. In 2000, Mr. Emad began his career in the Maintenance and Mechanical Division, working in the air-conditioning and refrigeration maintenance workshop. In 2004, he joined the Heat Exchangers Rehabilitation Unit within the Boilers and Furnaces Department. In 2013, he became the Head of the Heat Exchangers Rehabilitation Unit and the Deputy Director of the Boilers and Furnaces Department. Later, in 2020, he was appointed as the Director of the Boilers and Furnaces Department